How Does Polymorphism Affect the Interfacial Charge-Transfer States in Organic Photovoltaics?

Gabriele Boschetto,[†] Michal Krompiec,[‡,†] and Chris-Kriton Skylaris[*,†]

†*School of Chemistry, University of Southampton, Highfield, Southampton SO17 1BJ, United Kingdom*

‡*Merck Chemicals Ltd., Chilworth Technical Centre, University Parkway, Southampton SO16 7QD, United Kingdom*

E-mail: c.skylaris@soton.ac.uk

Phone: +44 (0)2380 599381

Abstract

The bulk heterojunction in organic photovoltaic (OPV) devices is a mixture of polymer (electron donor) and an electron acceptor material (typically functionalized fullerenes), and it is crucial for the device operation, as this is where excitons are split into electrons and holes to produce current. Non-fullerene acceptors (NFAs) are promising new materials for improving the device efficiency, and their solid-state arrangement with respect to the electron donor polymer is critical for the charge mobility and the performance of OPV devices. Although there have been numerous studies on NFAs, most of the current understanding comes from empirical considerations, with little atomistic-level interpretation of why and how the packing influences the charge transport properties of these materials. In this work we describe large-scale (with up to 3462 atoms) DFT simulations for ground and excited states on a number of polymer-NFA interfaces of realistic size, whose NFA domains consist of polymorphs of the same materials. Hence, we bridged the gap between experimental evidence and the intuitive expectation on the importance of intermolecular π-π stacking interactions in the NFA phase. We show that low connectivity leads to highly localized excitons, whereas in phases with a higher connectivity excitons are able to delocalize over multiple directions. Remarkably, excitons with a three-dimensional delocalization were also observed, leading to isotropic mobilities, similarly to fullerenes. Furthermore, a lower charge-transfer exciton binding energy and a lower energy loss between the lowest excitation of the polymer and the first charge-transfer state in the interface were both observed in systems characterized by a highly interconnected NFA phase. This suggests a higher probability of exciton splitting for these interfaces, which could potentially lead to higher device efficiencies.

Introduction

Non-fullerene acceptors (NFAs) have quickly replaced fullerenes in the state-of-the-art organic photovoltaic (OPV) devices: over the past few years reports of NFA-based modules

breaking the 10% performance barrier have significantly increased,[1–8] and power conversion efficiencies (PCEs) higher than 15%[9] and 17% (17.4% being the current reported performance record[10]) were also achieved, making OPV devices competitive against other photovoltaic technologies.

Among the pool of NFA materials, fused-ring electron acceptors (FREAs) show great promise, as they possess many advantages with respect to fullerenes, such as better tunability of the band gap, and a generally higher solubility, which is particularly important from a large-scale production point of view to significantly reduce the production costs with respect to fullerenes.[11]

Despite the numerous advantages, NFAs possess a bi-dimensional molecular geometry that in the solid state may hinder the mobility of the charge carriers, whereas the spherical shape of fullerenes (and their derivatives) allows three-dimensional percolation pathways, and thus high mobilities along the three dimensions, with values up to two orders of magnitude higher than typical FREA molecules.[12–14] The reason behind the difference in the performance does not only lie in their molecular shape, but also in their molecular packing in the solid state, as charge transport properties are generally understood to be significantly dependent on the molecular packing.[15–17] Particularly important for charge transport are the van der Waals interactions between the molecules in the crystal phase, with π-π stacking playing a crucial role: both the number and the strength of these interactions may favor the formation of charge transport pathways in the solid state.[18,19]

Structurally, FREAs are composed by a linearly fused aromatic central block (also known as the core), which is an electron-rich (donor) unit, with electron-poor (acceptor) blocks attached to both the ends of the core. Given their molecular structure, FREAs are also referred to as A-D-A molecules. Due to the presence of bulky alkyl side chains attached to the core, it is believed that strong π-stacking interactions in the crystal arrangement occur almost exclusively via the terminal acceptor moieties: this suggests that the charge transport pathways in the solid state are given by the orientation of these A-to-A close contacts.[20] Atomistic

molecular dynamics (MD) simulations on ITIC, one of the most popular NFA materials, underlined the importance of these A-to-A close contacts for an efficient charge transport.[21] Our meta-analysis on the molecular organization of non-fullerene acceptors[22] also corroborates this hypothesis via a thorough analysis of the topological connectivity, intermolecular close contacts, and charge transport density functional theory (DFT) calculations on a series of experimentally-determined NFA crystals. Charge carrier mobilities in the solid state were estimated by the calculation of electron effective masses, and results demonstrated that NFA crystals characterized by π-stacking interactions along the three dimensions show a more isotropic charge transport with respect to less interconnected packing arrangements.

Although important, these considerations do not take into account the presence of the donor phase (i.e., the π-conjugated polymer), as BHJs rely on the interaction between the electron acceptor and the electron donor materials. While there exists a large number of computational studies on the interaction between polymer and fullerenes,[23–27] the literature regarding the polymer-NFAs interaction is still limited. Few examples include the work of Wouk de Menezes et al.,[28] who carried out TDDFT calculations on small PTB7-th:ITIC interfaces to investigate the influence on the interfacial distance with respect to charge-transfer (CT) states, and the work of Shi et al.,[29] who explored the electron transfer of a p-DTS(FBTTh$_2$)$_2$:NIDCS-MO blend within the framework of semiclassical Marcus theory. Ab initio simulations on polymer-NFA interfaces are not trivial to perform, as it is not straightforward to understand how NFAs couple with the polymer. In addition, bulk heterojunctions are not easy to model with atomistic molecular simulations (such as DFT) due to their inherent complexity which would require, ideally, models composed of thousands of atoms, a number out of the reach of conventional DFT codes. To overcome this issue, we carried out ab initio simulations with the ONETEP code for linear-scaling DFT, which allowed us to study systems composed of more than 3000 atoms.

In this work we follow up on our aforementioned studies on the relationship between packing motif and mobility of NFA crystals, and we focus on the charge separation and

exciton dissociation step of the photovoltaic process in OPV. We coupled six different NFA crystals with a donor polymer, and we performed both ground- and excited-state calculations with DFT and TDDFT, respectively, focusing on the charge-transfer energies. We chose to consider two popular NFA molecules, ITIC[30] and 4TIC,[31] and for each of those we took three polymorphs, which by definition are characterized by the same molecular structure but arranged in different packing motifs, which could possibly also lead to different charge transport percolation pathways. We modelled the donor polymer as a derivative of PBTZT-stat-BDTT-8, a high-performing D-A copolymer developed by Merck.[32] By coupling this polymer with polymorphs of the same NFA molecules, we were not only able to investigate some of the aspects of the physics behind the CT process of fullerene-free BHJs, but also to explore the effect of different molecular arrangements on (i) the CT states of these interfaces, (ii) the exciton (de)localization, and (iii) the charge-transfer (CT) exciton binding energy ($E_{\mathrm{B}}^{\mathrm{CT}}$), i.e., the energy barrier that the exciton needs to overcome to split into a free electron and hole.

This work was enabled by the use of linear-scaling (TD)DFT with the ONETEP code, without which it would have been extremely challenging to consider NFA-polymer interfaces with the appropriate size and polymorphs. This study is organized as follows: in the following section (Methods) we present an overview of the concept behind linear-scaling DFT in the ONETEP code, and the setup details of our simulations (i.e., the computational parameters and a detailed description of our polymer-NFA models). The results of our simulations are then presented and discussed in Section 3, and conclusions are drawn in the final section.

Methods

ONETEP Program

ONETEP (Order-N Electronic Total Energy Package)[33] is an ab initio linear-scaling DFT code which allows $\mathcal{O}(N)$ scaling of the computational and memory calculation requirements

with respect to the total number of atoms N in the system of study, while ensuring at the same time near-complete basis set accuracy. ONETEP relies on the reformulation of density-matrix DFT: the conventional single-particle density matrix, $\rho(\mathbf{r}, \mathbf{r}')$, is re-expressed in the following separable form:

$$\rho(\mathbf{r}, \mathbf{r}') = \sum_{\alpha\beta} \phi_\alpha(\mathbf{r}) K^{\alpha\beta} \phi^*_\beta(\mathbf{r}') \tag{1}$$

where $\phi(\mathbf{r})$ are localized atom-centered orbital functions known as nonorthogonal generalized Wannier functions (NGWFs)[34] and K is density kernel. Note that this expression is equivalent to:

$$\rho(\mathbf{r}, \mathbf{r}') = \sum_{i} f_i \psi_i(\mathbf{r}) \psi^*_i(\mathbf{r}') \tag{2}$$

which is the conventional expression of the density matrix, where f_i is the occupancy of the state $\psi_i(\mathbf{r})$, a Kohn-Sham orbital function.

Linear-scaling behavior is achieved both by strictly localizing the NGWFs within a set radius and by spatial truncation of the density kernel K: these ensure sparsity of the density matrix $\rho(\mathbf{r}, \mathbf{r}')$. On the other hand, near-complete basis set accuracy is obtained through the self-consistent optimization of both the density kernel and the NGWFs during a calculation. In addition, by the expansion of the NGWFs in a basis of periodic sinc (psinc) functions,[35] ONETEP conveniently relies on the plane-wave formalism.

Simulation Details

Table 1: Overview of some of the relevant crystallographic information of the ITIC and 4TIC molecular crystals considered in this study.

backbone	CCDC no.	crystal system	space group	motif	π-π stacking
ITIC[21]	1575971	triclinic	$P\bar{1}$	herringbone	0D
ITIC[36]	1885952	triclinic	$P\bar{1}$	brickwork	2D
ITIC[22]	1942949	triclinic	$P\bar{1}$	brickwork	2D
4TIC[22]	1942947	monoclinic	$P2_1/c$	herringbone	0D
4TIC[22]	1942948	triclinic	$P\bar{1}$	brickwork	2D
4TIC[31]	1541584	triclinic	$P\bar{1}$	reticular	3D

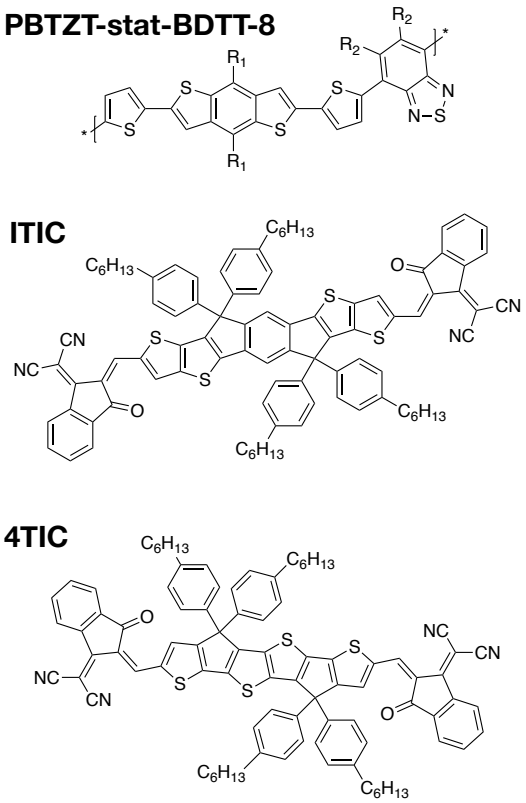

Figure 1: Molecular structure of the analogue of PBTZT-stat-BDTT-8 considered in this work, together with the non-fullerene acceptors ITIC and 4TIC.

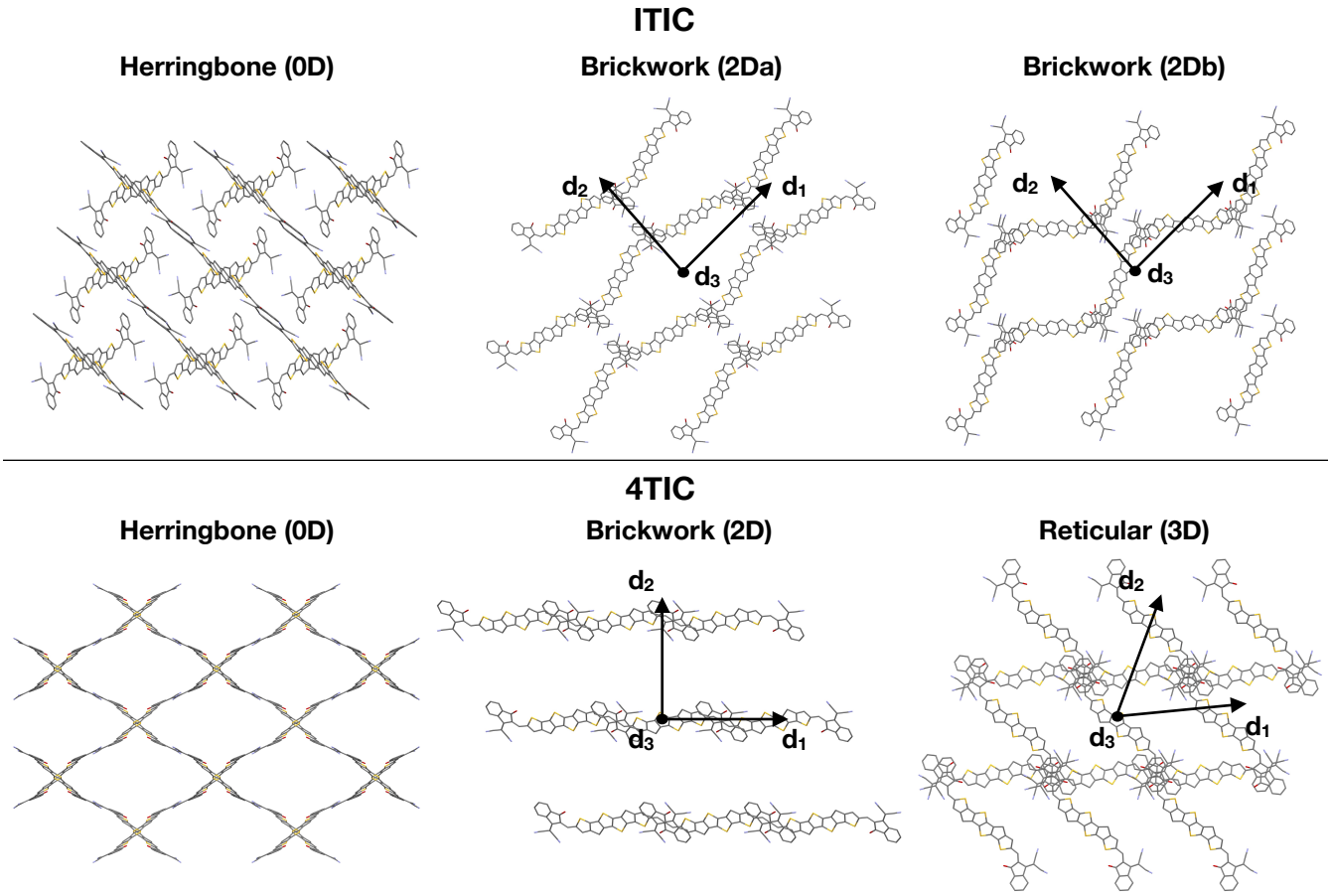

Figure 2: Molecular arrangements of the six molecular crystals used in this work. The directions of the interactions relevant for this study are also shown, with d_1 being orientated along the A-D-A backbones, d_2 being aligned along the separation distance between conducting planes of molecules, and d_3 being orientated along the cofacial π-stacking direction. Due to the higher geometrical complexity of reticular structures, d_1 and d_2 were defined as per figure. Herringbone structures by definition lack of strong π-stacking interactions along both d_1 and d_3, and there is no obvious way to define d_2: for these reasons no directions were shown in the figure. Hydrogens, side chains, and solvent molecules were hidden for clarity.

In this work we focused on the interaction between a model polymer and two NFA structures, ITIC and 4TIC, whose chemical structures are shown in Figure 1. The aim was to investigate with DFT and TDDFT simulations the influence of different ITIC and 4TIC packing motifs on the excited-state properties of polymer-NFA interfaces. We built our model polymer based on an analogue of PBTZT-stat-BDTT-8 (see Figure 1), and we modelled it as a linear alternating block copolymer composed of four A-D repeat units, with a total of 222 atoms. To model the NFA phase, we considered six experimentally-determined molecular crystals in total, three for both ITIC and 4TIC, each with a different packing motif. We point out that the three ITIC (and the three 4TIC) crystals are not all polymorphs sensu stricto, as in a few cases the side chains are either different or attached to the core in different positions. However, since this study is mainly focused on excited-state properties (which in general involve the A-D-A backbone only), and since some of the atoms present in the side chains were not properly resolved in the X-ray diffraction (XRD) analyses, we removed all the side chains. Moreover, since the presence of solvent molecules in some crystals was masked due to, once again, a poor resolution of their atomic positions in the XRD analyses, solvent molecules were also eliminated. This led to three crystals of ITIC and three crystals of 4TIC containing the atomic positions of the A-D-A backbones only, and therefore from this point onwards we will refer to these as polymorphs, as the backbones are the same for each set of structures.

Table 1 shows an overview of some of the relevant crystallographic information of both ITIC and 4TIC molecular crystals, and particularly important for this work are the packing motif and the π-stacking dimensionality. The latter is defined as the dimensionality of the π-π overlap between the terminal units of each NFA molecule in the crystal, in other words, the acceptor-to-acceptor (A-to-A) close contacts. For a more detailed discussion on the packing dimensionalities and the corresponding charge percolation pathways, the reader is referred to our meta-analysis on the molecular organization of non-fullerene acceptors.[22] Examples of the packing arrangements are shown in Figure 2: as it can be observed, a 0D herringbone

packing motif is characterized by no (or very weak) A-to-A π-π contacts, whereas both 2D and 3D motifs allow multiple A-to-A close contacts along different directions. Particularly interesting is the reticular 3D packing, in which, despite the flat bi-dimensional structure of A-D-A molecules, the π-π contacts in the solid state allow, in principle, a more isotropic charge transport in the three dimensions, thus potentially overcoming the main issue of NFAs with respect to fullerenes. In principle, the 2D brickwork arrangement, as the name suggests, allows charge percolation pathways along two directions only, that is, along the molecule backbone (d_1) and through the A-to-A π-stacking direction (d_3); however, a more twisted arrangement of the molecules along d_1 could lead to interactions also along d_2, as in the case of the two brickwork ITIC polymorphs: in both structures the intermolecular distance along d_2 is, in some cases, less or close to 3.5 Å (see Figure S1 and S2 for more details). Moreover, in the more twisted polymorph some A-to-D close contacts can also be observed (Figure S2), and we would expect an even stronger interaction between planes along d_2. Indeed, even though from a geometrical point of view the crystal arrangement is brickwork, our previous calculations suggested that, in terms of mobility, the material behaves like a reticular 3D structure.

With the aim of building NFA phases representative of the aforementioned π-stacking dimensionalities in the solid state, we cut suitably large sections of each solid, and we obtained three ITIC-based crystal sections with 24 molecules in total, whereas in the case of 4TIC we obtained three crystal sections composed of 30 molecules. We cut these sections in such a way that for each of those only three A terminal groups were able to interact with the polymer chain in a face-to-face π-stacking arrangement; the intermolecular distance between the polymer and the NFA phase was set to 3.4-3.5 Å, and this value was obtained by performing some exploratory calculations on a small 1-to-1 composite (details of this will be presented below). We stress here that there exist many different ways in which the sections could have been extracted from each crystal, and also many ways in which the NFA and the polymer phases could have been coupled. For these reasons, the strategy that we used

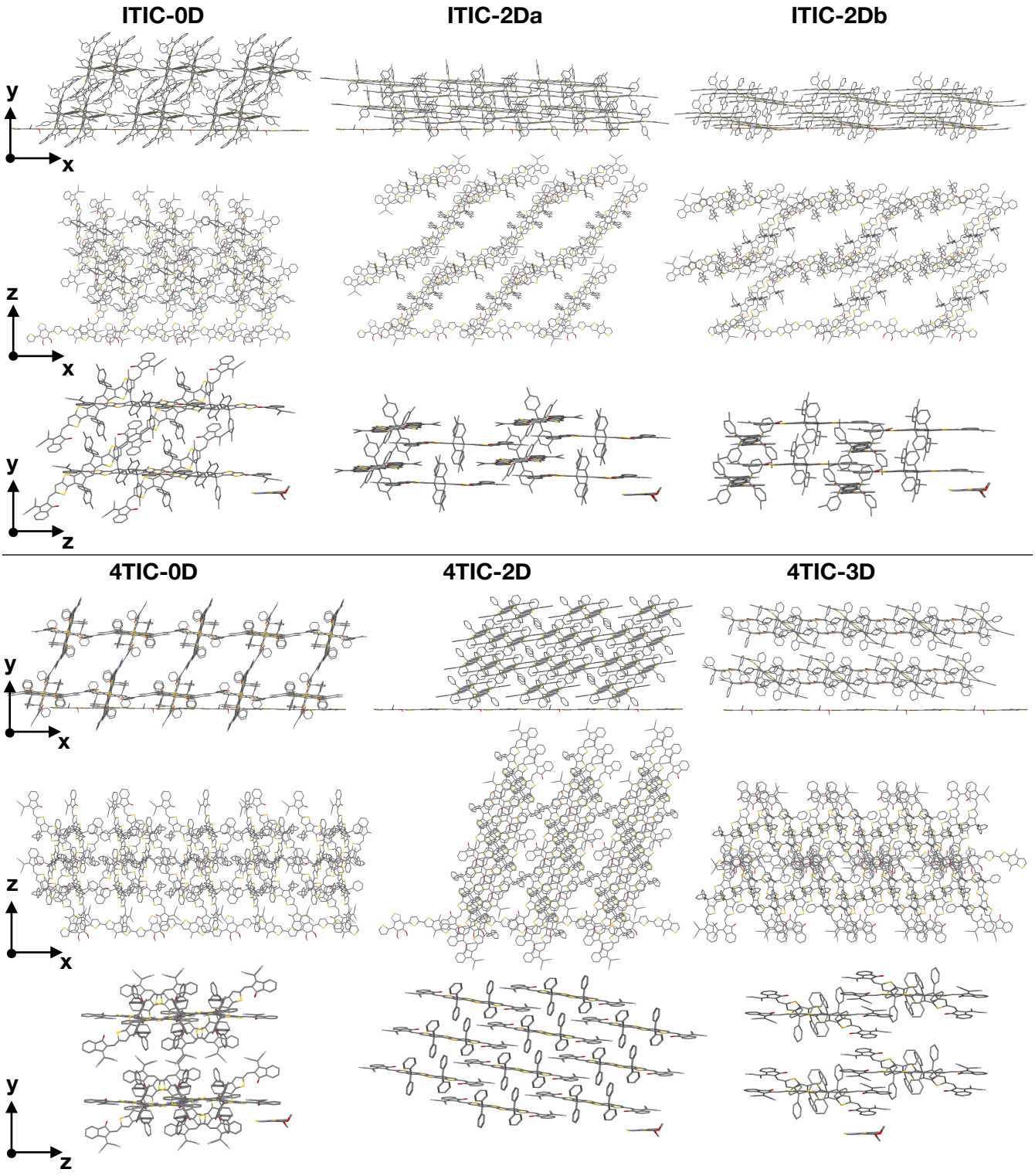

Figure 3: Structures of the ITIC and 4TIC interfaces with polymer constructed and studied in this work. Hydrogen atoms were hidden for clarity.

to extract the NFA sections and to construct the interfaces was to ensure full comparability of results between polymorphs: each ITIC (4TIC) interface consists of the same number of atoms and molecules, and both the interphase distance and the number of interactions with the polymer are also the same. The resulting ITIC-based and 4TIC-based interfaces, whose structures are shown in Figure 3, are composed of 3246 and 3462 atoms each, respectively. From this point onwards we will refer to each interface as the name of the NFA molecule and the dimensionality of the π-stacking network, e.g., 4TIC-0D, 4TIC-2D, and 4TIC-3D, as the polymer molecule does not change. To distinguish the two ITIC brickwork motifs we will use the 2Da and 2Db nomenclature, and the corresponding interfaces will be ITIC-2Da and ITIC-2Db (see Figure 2 and 3).

Ground- and excited-state calculations were performed with the ONETEP code using the Perdew-Burke-Ernzerhof (PBE) exchange-correlation functional[37] and norm-conserving pseudopotentials to model core electrons. Dispersion interactions were taken into account by including the empirical D2 dispersion correction by Grimme.[38] A psinc kinetic energy cutoff of 800 eV was used, and the NGWFs radius was set to 9.0 bohr for every atomic species. We used 4 NGWF functions for the C, N, O, S atoms, and 1 for H atoms. These settings were used in single-point, conduction bands optimization,[39] and full TDDFT[40] calculations. All simulations were performed in the vacuum and at the Γ-point only. We note that no geometry relaxation was performed on the atomic positions of the NFA phases in the large interfaces, the only exception being the hydrogen atoms, whose atomic coordinates were adjusted with the software Materials Studio.[41] This was done not to disrupt the arrangement of the backbones in the solid state, which would lead to different crystal packings with respect to the experimental structures, and to ensure that the simulations were carried out on experimental data only. A geometry optimization was performed only on a small 1-to-1 dimer-NFA model composite, to obtain the optimal interphase distance, and this was carried out with ONETEP by using the same parameters outlined above. Since at present only nonhybrid functionals are available in ONETEP for TDDFT calculations, excited-state

simulations on the large interfaces were performed using the PBE functional, which is known to have some limitations when describing CT states (the energies of this type of transitions are generally underestimated). However, we also note that calculations on polymer-NFA interfaces of this size have never been performed with ab initio methods, to the best of our knowledge; moreover, we expect that qualitative results can be obtained also with GGA functionals. Nevertheless, to investigate the behaviour of GGAs against hybrid functionals, we performed a set of exploratory calculations on a small 1-to-1 model composite: TDDFT calculations were performed with Gaussian 09[42] using both PBE and B3LYP[43,44] functionals with the def2-SVP basis set,[45,46] and results in terms of ground-to-excited-state density difference map were compared.

Exploratory investigation of small 1-to-1 polymer-ITIC composites

Modelling a polymer is relatively straightforward, however, modelling the NFA phase is a more challenging task, since large NFA domains consisting of more than a few molecules are required in order to represent crystal polymorphs correctly. In addition, the flat bi-dimensional geometric shape of common A-D-A NFAs adds an additional layer of complexity when modelling this class of materials, since, as opposed to fullerenes, there is no obvious way to stack a NFA molecule on top of a polymer chain. For these reasons, we first focused on a small composite model system, and the results obtained aided in the design of the much larger interfaces. The 1-to-1 model was composed of a PBTZT-stat-BDTT-8 dimer and one molecule of ITIC.

We first investigated the packing arrangement by computing the polymer-NFA composite binding energy (E_{B}), defined as:

$$E_{\mathrm{B}} = E^{\mathrm{PN}} - (E^{\mathrm{P}} - E^{\mathrm{N}}) \tag{3}$$

where E^{PN} is the total energy of the whole composite, whereas E^{P} and E^{N} are the total

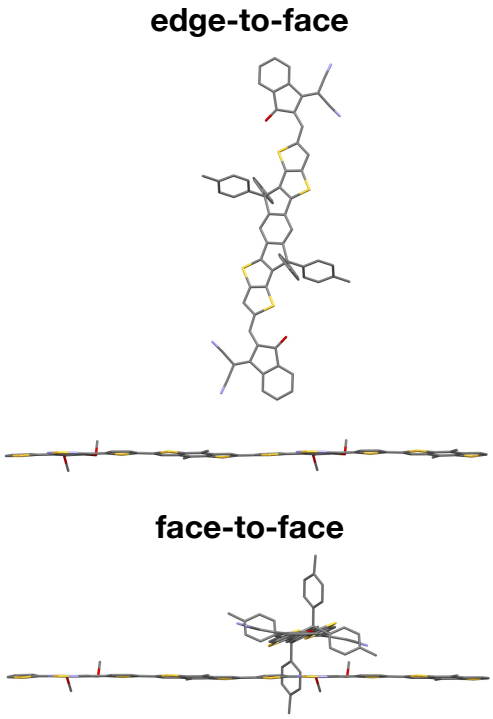

Figure 4: Structure of the two limiting cases of the stacking arrangement of ITIC-polymer composite, face-to-face and edge-to-face. Hydrogen atoms were hidden for clarity.

energies of the polymer chain and the NFA phase (in this case one single ITIC molecule), respectively. We chose to explore two limiting cases, that is, a face-to-face and an edge-to-face arrangement (see Figure 4) and we paired ITIC with the dimer by coupling the acceptor block of the dimer with the terminal acceptor group of ITIC. We chose this positioning for two reasons: on the one hand, previous studies suggested that the electron-acceptor phase tends to couple more efficiently with D-A polymers when it interacts with their A blocks (higher PCEs are generally observed),[47] whereas, on the other hand, the presence of the bulky alkyl side chains in the central D unit of ITIC (but also 4TIC) is likely to cause a significant steric hindrance, essentially leaving only the ITIC acceptor terminal groups sterically available. Calculations on E_{B} showed that the face-to-face arrangement is significantly more favored than the edge-to-face, as the composite binding energy is roughly six times stronger (0.6 eV against 0.09 eV): this is not entirely unexpected since, intuitively, in a face-to-face arrangement both molecules are able to interact via a cofacial π-π stacking, whereas

in the edge-to-face case the portion of ITIC interacting with the dimer is much smaller. A subsequent geometry relaxation of the small face-to-face model composite showed that the optimal stacking distance is 3.4-3.5 Å, in agreement with previous computational studies on small polymer-NFA composites.[28,48]

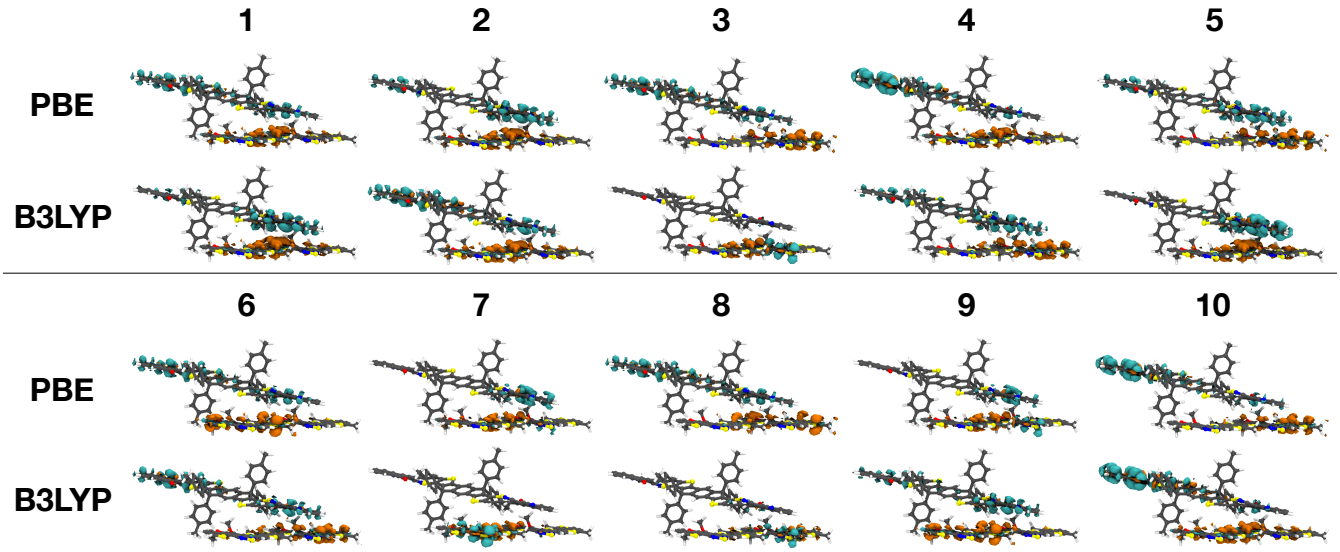

Figure 5: Comparison between PBE and B3LYP EDD maps of each computed TDDFT transition of the face-to-face dimer/ITIC model composite. Charge accumulation is shown in cyan, whereas charge depletion in orange.

TDDFT calculations on the face-to-face composite were performed, and we computed the first 10 excited states. For each state we then plotted the ground-to-excited-state electron density difference (EDD) map, and results were compared between PBE and B3LYP functionals. As shown in Figure 5, EDD maps are qualitatively not dissimilar between the GGA and the hybrid functional, to some extent: for instance, states 1, 2, 4, 5, 6, and 10 all have a CT character with both functionals. However, as expected, PBE predicts a higher number of CT states in the low-energy part of the spectrum and before the dimer first excited state (S_1), whereas with B3LYP we were able to assign two CT states which were ∼0.3 eV lower in energy than the dimer S_1 state. We calculated the energy difference between the PBE first CT state and the corresponding B3LYP CT state, which is 0.69 eV. We then used this value to rigidly shift and correct the excited state transition energies of the large ITIC- and

4TIC-based interfaces, to overcome the systematic GGA underestimate of CT energies and to rescale those with respect to B3LYP. We assumed that, given the significantly smaller energy range in which the computed excited states of the large interfaces lied with respect to the 1-to-1 composite (∼3-4 times smaller than 0.3 eV), and given the fact that these states all had a CT character, PBE and B3LYP would lead to qualitatively similar TDDFT results in terms of exciton electron and hole densities. However, we note that when computing the charge-transfer exciton binding energies ($E_{\mathrm{B}}^{\mathrm{CT}}$) no shift was applied; we estimated $E_{\mathrm{B}}^{\mathrm{CT}}$ via the following equation:[49]

$$E_{\mathrm{B}}^{\mathrm{CT}} = E_{\mathrm{CS}} - E_{\mathrm{CT_1}} = (\mathrm{IP} - \mathrm{EA}) - E_{\mathrm{CT_1}} \tag{4}$$

in which E_{CS} is the energy of the charge-separated state, which can be estimated as the difference between the ionization potential (IP) and the electron affinity (EA) of the polymer and the NFA in the interface, respectively;[50] IP and EA were computed via a ΔSCF procedure. Finally, $E_{\mathrm{CT_1}}$ is the energy of the lowest interfacial CT state.

Results and Discussion

Calculations showed that different packing motifs of the NFA phase affect the ground-state properties of this class of materials, as can be observed from Figure 6, which shows the density of states (DOS) of both ITIC- and 4TIC-based interfaces, together with the local DOS (LDOS) projected on the polymer chain. Generally, the polymer has a very small contribution to the total DOS, and this is due to its limited size if compared to all NFA domains (∼200 atoms against ∼3000 atoms); moreover, its LDOS shows little to no difference regardless of the NFA phase it is coupled with. We conclude that the changes in the total DOS can be attributed almost exclusively to the polymorphism of the NFA phase. For both ITIC and 4TIC class of interfaces, differences in the DOS can be observed at both lower and higher energies with respect to the Fermi level, and this suggests that NFA polymorphism

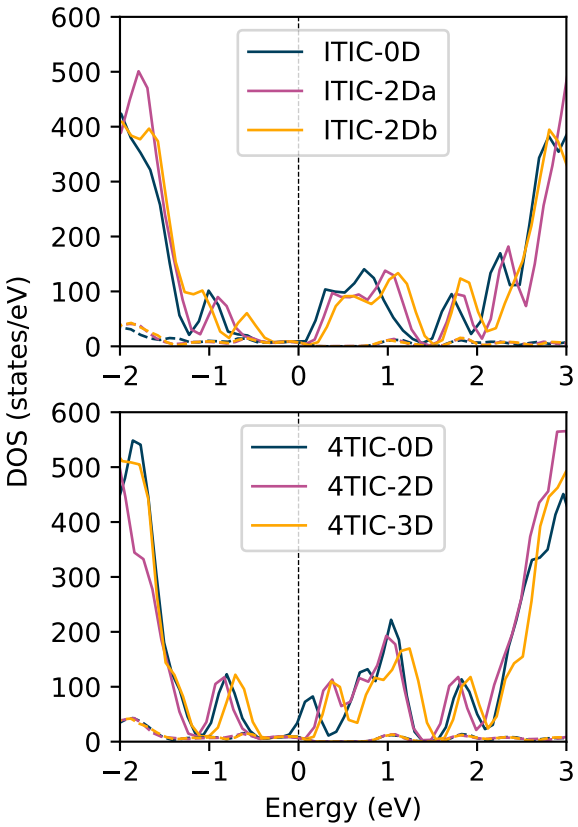

Figure 6: DOS of the six NFA-polymer inerfaces considered in this work. For each interface the total DOS (full line) and the local DOS projected on the polymer chain (dashed line) are shown. The DOS were centered around the Fermi level of each interface, and a Gaussian smearing of 0.1 eV was applied.

affects both the valence and the conduction bands of the whole interface. For instance, while the edges of the first conduction bands of 4TIC-2D and 4TIC-3D almost overlap, the conduction band edge of 4TIC-0D occurs at lower energies; a similar trend is also found in the ITIC-based interfaces. As a consequence, we expect also the band gap of the whole interfaces to be virtually affected by the NFA polymorphism, and indeed this is confirmed by our results, which show an increasing trend that can be linked to the increased π-stacking dimensionality of the NFA phase. We found an increase of 0.1 eV in the ITIC interfaces, and about 0.25 eV in the 4TIC-based structures.

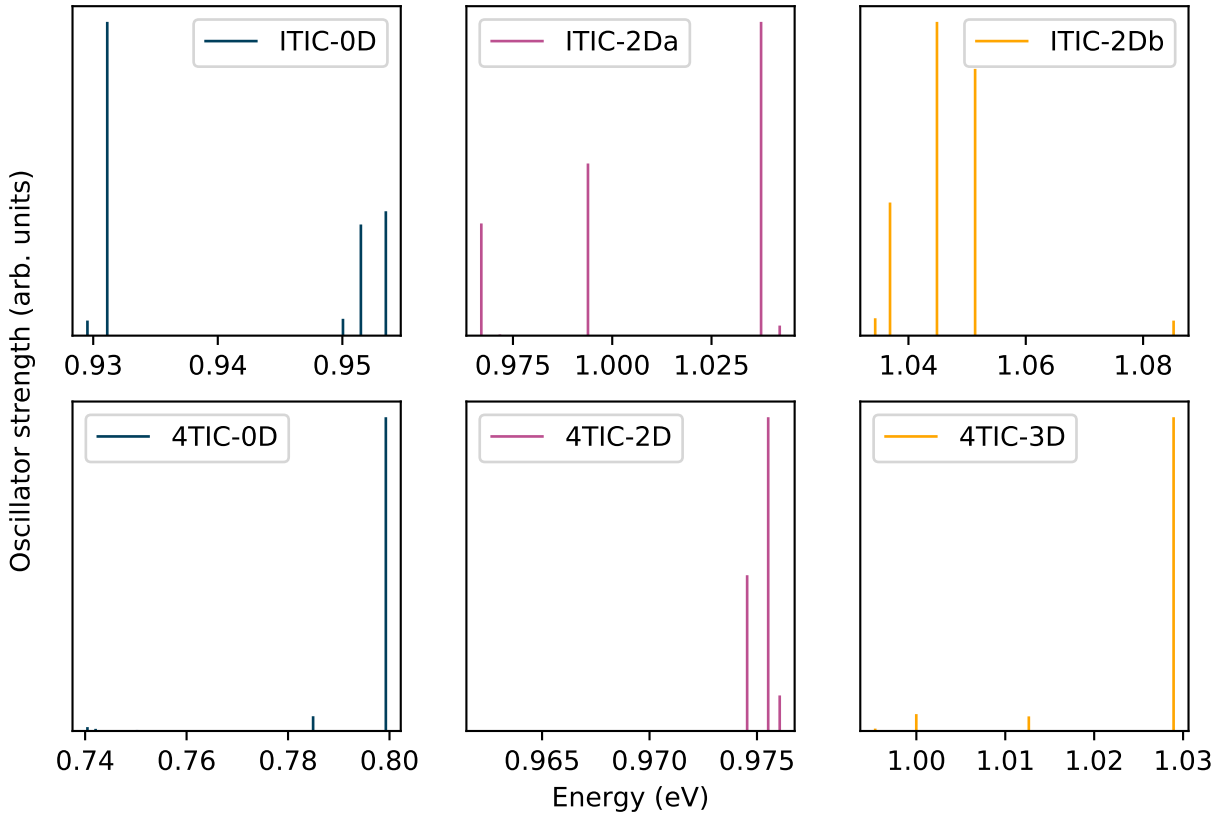

Figure 7: Comparison between excited-state spectra of ITIC- (top three plots) and 4TIC-based (bottom three plots) interfaces. A rigid shift was applied to each plot to correct the values of the transition energies with respect to B3LYP, as previously discussed.

We then performed TDDFT calculations on each interface, and we computed the first 5 excited states. These were all found to have a CT character, since each state involved a transition from the polymer to the NFA domain. A breakdown of every transition is shown

Table 2: Breakdown of the first five CT states for each of the ITIC- and 4TIC-based interfaces considered in this work.[a]

	ITIC			4TIC		
CT	0D	2Da	2Db	0D	2D	3D
1	H → L	H → L	H → L	H → L	H → L	H → L
2	H → L+1	H → L+1	H → L+1	H → L+1	H → L+1	H → L+1
3	H → L+2	H → L+2	H → L+2	H → L+2	H → L+2	H → L+2
4	H → L+3	H → L+3	H → L+3	H → L+3	H → L+3	H → L+3
5	H → L+4 (0.89)	H → L+4 (0.81)	H → L+4	H → L+4 (0.94)	H → L+4	H → L+4 (0.58)
	H → L+5 (0.10)	H → L+5 (0.18)		H → L+5 (0.05)		H → L+5 (0.42)

[a] Note that every transition has a charge transfer character, and therefore every electron-donating orbital (H) is located on the oligomer while every electron-accepting orbital (L) is located on the NFA phases.

in Table 2, in which it can be seen that each of those occurs from the HOMO level of the polymer to the LUMOs of the NFA domain. In addition, most of the CT states have a pure HOMO → LUMO character, however, CT_5, which is the energetically highest CT state, shows a mixed character in the majority of the interfaces. Figure 7 shows the excited-state spectra of both ITIC- and 4TIC-based interfaces, obtained with TDDFT: for both these types of materials the CT energies are affected by the polymorphism of the NFA phase, in line with our previous results in the ground state. It appears that the higher the π-stacking dimensionality is, the higher the energy of the transitions becomes, that is, 0D → 2D → 3D. Moreover, it is clear that this effect is non-negligible, as for ITIC we observe a shift of ∼0.10 eV in the energy of the lowest CT state (CT_1), whereas for 4TIC this shift is more intense, on the order of ∼0.25-0.30 eV. This is quite remarkable, since, as previously discussed, interfaces are constructed in the same way, and the only factor which differs is the packing motif of the NFA domain. This implies that the excess energy (i.e., the energy loss resulting from the exciton generation upon photoabsorption in the polymer phase) is lower when the NFA domain is more interconnected, as this quantity is essentially the difference between the first singlet state S_1 of the polymer and the CT_1 state of the polymer-NFA interface. We note that this excess energy would dissipate into heat, and therefore it would be essentially wasted, as shown by recent experimental studies.[51–53] Moreover, a minimization of this quantity leads

to an increased PCE towards the Shockley–Queisser limit.[54]

We also investigated the effect of polymorphism on the charge-transfer exciton binding energy ($E_{\mathrm{B}}^{\mathrm{CT}}$) of the interfaces. We computed $E_{\mathrm{B}}^{\mathrm{CT}}$ for each of the interfaces studied in this work, and results suggested that polymorphism does significantly have an impact on this quantity as well. We found that the higher the π-stacking dimensionality is, the lower $E_{\mathrm{B}}^{\mathrm{CT}}$ becomes: in the case of ITIC interfaces, binding energies were found to be 1.10 eV, 0.80 eV, and 0.71 eV for ITIC-0D, ITIC-2Da, and ITIC-2Db, respectively, whereas in the case of 4TIC interfaces, values were 0.38 eV for both 4TIC-0D and 4TIC-2D, and 0.25 for 4TIC-3D. This significant decrease in $E_{\mathrm{B}}^{\mathrm{CT}}$ can be linked to a higher delocalization of the CT states of both ITIC-2Db and 4TIC-3D which favors the hole-electron splitting, as it increases the exciton separation distance. This is corroborated by the exciton hole and electron density plots, which will be discussed below. We note that $E_{\mathrm{B}}^{\mathrm{CT}}$ is strongly material-dependent, and this justifies the different values between ITIC- and 4TIC-based interfaces. However, we point out that the trend is the same for both types of interfaces. We also note that the estimated $E_{\mathrm{B}}^{\mathrm{CT}}$ are not too dissimilar from experimental results on organic semiconductors.[49,55]

Interestingly, we note that both the exciton binding energy and the excess photon energy decrease when the dimensionality of the π-π network increases, and this strongly suggests that the probability of exciton splitting is much higher in polymer-NFA interfaces composed of highly interconnected NFA domains.

Finally, fundamental to the understanding of the physics of charge transfer are the exciton hole and electron density plots, which can be obtained with TDDFT and are shown in Figure 8 and Figures S3-S20. We note that the plots of both ITIC- and 4TIC-based interfaces confirm that all the computed transitions have a charge-transfer character, since the exciton hole density is always localized on the polymer chain only, whereas the exciton electron density is always found on the NFA phase exclusively. Notably, the (de)localization of the electron densities seems to depend significantly on the π-stacking dimensionality of the NFA domain, and in other words, on polymorphism, at least for the materials taken into

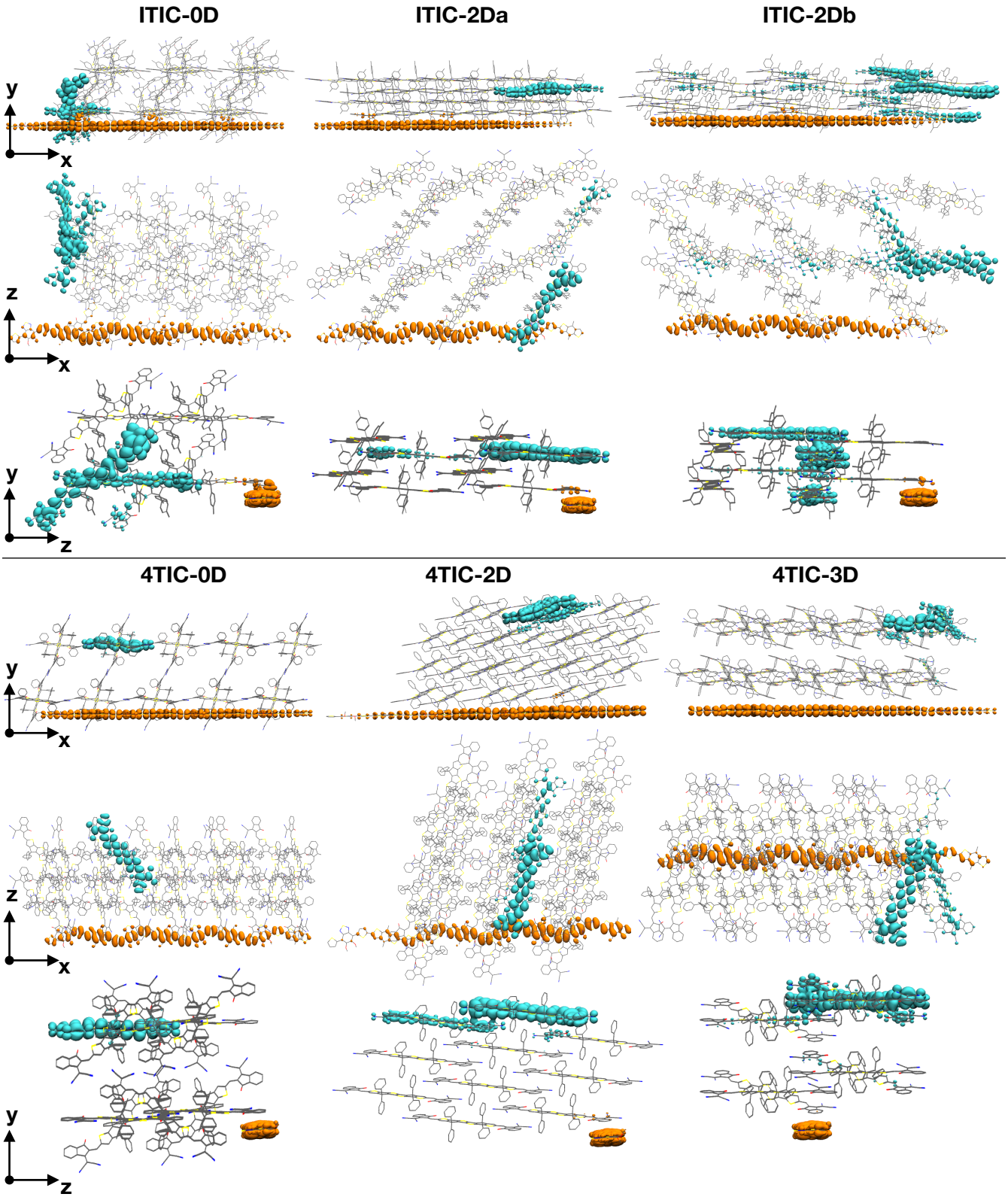

Figure 8: Exciton hole and electron density plots relative to the first CT state (CT_1) of the ITIC- and 4TIC-based interfaces. The exciton electron density is shown in cyan, whereas the exciton hole density in orange. Hydrogen atoms were hidden for clarity.

consideration in this work: both ITIC-0D and 4TIC-0D are characterized by rather localized transitions, the exciton electron density involving clusters of two/three near molecules for ITIC-0D, and only one single molecule for 4TIC-0D. These results suggest that the lack of strong π-π interactions between the NFA molecules (in particular cofacial A-to-A π-stacking) leads to localized excitons, which strongly hinders charge transport, and consequently, also device performance. It is important to point out that this does not necessarily mean that molecules with a herringbone packing motif do not interact and/or possess near-zero mobilities, but we would expect these to perform worse than molecules arranged with higher connectivities. This is confirmed by Han et al., which estimated the average mobility of the herringbone ITIC to be significantly lower than the average mobility of a more interconnected ITIC arrangement.[21] We also note that the interaction strength also strongly depends on the chemical nature of the molecule itself: for instance, the CT transitions of 4TIC-0D are significantly more localized than ITIC-0D, and we would probably expect a worse average electron mobility for the first.

The brickwork arrangement would allow, in principle, for charge percolation pathways along two directions, and this is particularly visible in the electron densities of 4TIC-2D: in fact, it is possible to observe that most of the states delocalize along the 4TIC backbone (direction d_1, as previously defined and shown in Figure 2) and also along the perpendicular π-stacking direction (d_3 in Figure 2). Consistently with the packing motif, no CT state shows delocalization along the d_2 direction, as the molecules are too far away to be able to interact. Contrary to this, the exciton electron densities of ITIC-2Da also extend over molecules belonging to different conducting planes along d_2. As previously discussed, this is the result of the backbone twisting along d_1. We also note that the only state whose delocalization is significant is the highest CT_5: we attribute this behavior to the fact that this is an energetically high-lying CT state, and we expect it to be more delocalized.[56]

Particularly interesting are the electron densities of ITIC-2Db and 4TIC-3D, as results show that these are both more delocalized with respect to their counterparts, and this is

consistent with our calculations of effective masses, which showed very good (in the case of ITIC-2Db), and good (in the case of 4TIC-3D) mobilities along d_1, d_2, and d_3. ITIC-2Db presents electron densities that are delocalized over multiple molecules, and along the three dimensions of the NFA phase; 4TIC-3D, although been less delocalized, also presents electron densities that span the three dimensions. We note that this is once again consistent with our previous calculations, which showed that 4TIC-3D performs worse than ITIC-2Db in terms of effective masses. We stress here that a 3D molecular arrangement does not ensure necessarily to achieve high mobilities and high device performances: for instance, we found that the average effective mass of 4TIC-3D is still more than double the average mass of ITIC-2Db (0.88 m_e against 0.40 m_e), although we would expect a better performance if compared to 0D materials, and a large part of 2D materials. What does matter is that in principle an interconnected packing motif allows delocalized electron densities and isotropic mobilities, which are both typical of fullerene crystals. Nevertheless, we point out that although we generally observed an increased delocalization of the exciton with respect to the π-stacking dimensionality, calculations on polymer-fullerene large interfaces showed that the exciton electron density of fullerenes is still significantly more delocalized than the highly interconnected crystals considered in this work, as fullerenes are inherently symmetrical molecules.[57] However, we showed that by acting on their crystal packing only, the anisotropic behavior of NFAs can be significantly reduced.

Conclusions

The active layer in OPV devices is the bulk heterojunction, which is a mixture of polymer (electron donor) and an electron acceptor material (typically functionalized fullerenes), and it is crucial for the device operation, as this is where excitons are split into electrons and holes to produce current. Non-fullerene acceptors are promising new materials for improving the device efficiency, and their solid-state arrangement with respect to the electron donor

polymer is critical for the charge mobility and the performance of OPV devices. In order to understand the importance of the solid-state arrangement, we performed large-scale (with up to 3462 atoms) DFT and TDDFT simulations on a number of polymer-NFA interfaces of realistic size, whose NFA domains consisted of polymorphs of the same materials. We investigated the role of molecular packing on two sets of model interfaces, constructed by coupling a polymer with three ITIC and 4TIC crystal polymorphs with different degrees of π-π connectivity.

We found that polymorphism strongly affects both the electronic and optical properties of polymer-NFA interfaces. In terms of ground-state properties, we found that both the valence and the conduction bands, as well as the band gap, are significantly affected: more specifically, a more interconnected π-stacking network causes an increase of the band gap, which correlates with the change in the valence and conduction bands around the Fermi level.

In terms of excited-state properties, polymorphism significantly affects both the energy and the localization of the charge transfer states. We found that a higher connectivity of the NFA phase correlates with a non-negligible upward shift (up to $\sim$0.3 eV in the case of 4TIC-based interfaces) of the energy of the first charge transfer state CT_1, which leads to a lower excess energy (i.e., the energy loss between the lowest excitation of the polymer and the first charge-transfer state in the interface). We also found that the CT exciton binding energy decreased by 0.4 eV from ITIC-0D to ITIC-2Db, whereas in 4TIC-based interfaces the difference was $\sim$0.15 eV. Both these results point in the direction of a higher exciton splitting probability in interfaces characterized by NFA phases with high π-stacking connectivities.

The TDDFT electron-hole density plots confirmed that the computed states had all a polymer-to-NFA charge transfer character, as the exciton hole density was localized exclusively on the polymer chain, whereas the exciton electron density was found exclusively on the NFA domain. By investigating the spatial localization of the exciton electron density on the different NFA domains we were also able to qualitatively explain how the stacking of

π-conjugated motifs determines charge transport. We found that if the π-stacking dimensionality is low, as in the case of the herringbone packing, the exciton electron density is localized. For these interfaces we would expect generally low and strongly anisotropic total mobilities, as no continuous charge percolation pathways were observed; previous studies on ITIC confirm this hypothesis.[21] On the contrary, we found that highly interconnected packing motifs, such as the reticular 4TIC-3D, lead to a higher degree of delocalization of the exciton electron density along the three dimensions, similarly to what we observed on fullerene clusters in our previous work,[57] and therefore we expect a more isotropic mobility. Brickwork packing motifs showed an intermediate behavior in terms of exciton electron density (de)localization, and we attributed this to the twisting angle of the molecules stacked along the d_1 direction (roughly parallel to the backbone). For instance, the charge-transfer states of 4TIC-2D delocalize over the d_1 and d_3 directions, but never along the d_2 direction, as the corresponding intermolecular distance is high. In the case of ITIC-2Da we observed a similar behavior, but given the shorter intermolecular distance along d_2, we found that the exciton electron density could, in some cases, delocalize along that direction too. Finally, ITIC-2Db is characterized by a more significant twisting angle, and that led to a high molecular interconnection between conducting planes, reflected by the exciton electron density which delocalizes along the three dimensions like in a reticular packing motif.

This study provided important insights into the properties of polymer-acceptor interfaces and into the importance of the molecular packing of non-fullerene acceptors, and contributes towards the design and commercialization of high-performing fullerene-free OPV devices. We expect our results to be useful in this sense, and we hope these would further inspire research towards optimal crystal engineering of NFAs.

Acknowledgement

The authors would like to thank Pierluigi Mondelli for providing some of the crystal struc-

tures necessary to the scope of this work. G. B. also thanks both Merck and EPSRC for supporting his Ph.D. studentship via a Doctoral Training Centre Grant (no. EP/L015382/1). We are grateful for access to the Iridis5 Supercomputer of the University of Southampton. We are also grateful for computational support from the UK national high performance computing service, ARCHER, for which access was obtained via the UKCP consortium and funded by EPSRC grant ref EP/P022030/1.

Supporting Information Available

Images of the intermolecular close contacts of ITIC-2Da and ITIC-2Db NFA phases. Exciton hole and electron density plots of the higher CT states of the ITIC- and 4TIC-based interfaces considered in this work. Atomic coordinates of the large interfaces constructed for this study.

References

(1) Wadsworth, A.; Ashraf, R. S.; Abdelsamie, M.; Pont, S.; Little, M.; Moser, M.; Hamid, Z.; Neophytou, M.; Zhang, W.; Amassian, A. et al. Highly Efficient and Reproducible Nonfullerene Solar Cells from Hydrocarbon Solvents. *ACS Energy Lett.* **2017**, *2*, 1494–1500.

(2) Liu, F.; Zhou, Z.; Zhang, C.; Vergote, T.; Fan, H.; Liu, F.; Zhu, X. A Thieno[3,4-b]thiophene-Based Non-Fullerene Electron Acceptor for High-Performance Bulk-Heterojunction Organic Solar Cells. *J. Am. Chem. Soc.* **2016**, *138*, 15523–15526.

(3) Li, Z.; Jiang, K.; Yang, G.; Lai, J. Y. L.; Ma, T.; Zhao, J.; Ma, W.; Yan, H. Donor Polymer Design Enables Efficient Non-Fullerene Organic Solar Cells. *Nat. Commun.* **2016**, *7*, 13094.

(4) Li, S.; Ye, L.; Zhao, W.; Zhang, S.; Mukherjee, S.; Ade, H.; Hou, J. Energy-Level

Modulation of Small-Molecule Electron Acceptors to Achieve over 12% Efficiency in Polymer Solar Cells. *Adv. Mater.* **2016**, *28*, 9423–9429.

(5) Zheng, Z.; Awartani, O. M.; Gautam, B.; Liu, D.; Qin, Y.; Li, W.; Bataller, A.; Gundogdu, K.; Ade, H.; Hou, J. Efficient Charge Transfer and Fine-Tuned Energy Level Alignment in a THF-Processed Fullerene-Free Organic Solar Cell with 11.3% Efficiency. *Adv. Mater.* **2017**, *29*, 1604241.

(6) Zhao, W.; Li, S.; Yao, H.; Zhang, S.; Zhang, Y.; Yang, B.; Hou, J. Molecular Optimization Enables over 13% Efficiency in Organic Solar Cells. *J. Am. Chem. Soc.* **2017**, *139*, 7148–7151.

(7) Yang, Y.; Zhang, Z.-G.; Bin, H.; Chen, S.; Gao, L.; Xue, L.; Yang, C.; Li, Y. Side-Chain Isomerization on an n-type Organic Semiconductor ITIC Acceptor Makes 11.77% High Efficiency Polymer Solar Cells. *J. Am. Chem. Soc.* **2016**, *138*, 15011–15018.

(8) Li, Y.; Zhong, L.; Gautam, B.; Bin, H.-J.; Lin, J.-D.; Wu, F.-P.; Zhang, Z.; Jiang, Z.-Q.; Zhang, Z.-G.; Gundogdu, K. et al. A Near-Infrared Non-Fullerene Electron Acceptor for High Performance Polymer Solar Cells. *Energy Environ. Sci.* **2017**, *10*, 1610–1620.

(9) Yuan, J.; Zhang, Y.; Zhou, L.; Zhang, G.; Yip, H.-L.; Lau, T.-K.; Lu, X.; Zhu, C.; Peng, H.; Johnson, P. A. et al. Single-Junction Organic Solar Cell with Over 15% Efficiency Using Fused-Ring Acceptor with Electron-Deficient Core. *Joule* **2019**, *3*, 1140–1151.

(10) Meng, L.; Zhang, Y.; Wan, X.; Li, C.; Zhang, X.; Wang, Y.; Ke, X.; Xiao, Z.; Ding, L.; Xia, R. et al. Organic and Solution-Processed Tandem Solar Cells with 17.3% Efficiency. *Science* **2018**, *361*, 1094–1098.

(11) Anctil, A.; Babbitt, C. W.; Raffaelle, R. P.; Landi, B. J. Material and Energy Intensity of Fullerene Production. *Environ. Sci. Technol.* **2011**, *46*, 2353–2359.

(12) Zhang, L.; Lin, B.; Ke, Z.; Chen, J.; Li, W.; Zhang, M.; Ma, W. A Universal Approach to Improve Electron Mobility Without Significant Enlarging Phase Separation in IDT-Based Non-Fullerene Acceptor Organic Solar Cells. *Nano Energy* **2017**, *41*, 609–617.

(13) Zhang, J.; Tan, H. S.; Guo, X.; Facchetti, A.; Yan, H. Material Insights and Challenges for Non-Fullerene Organic Solar Cells Based on Small Molecular Acceptors. *Nat. Energy* **2018**, *3*, 720–731.

(14) Wadsworth, A.; Moser, M.; Marks, A.; Little, M. S.; Gasparini, N.; Brabec, C. J.; Baran, D.; McCulloch, I. Critical Review of the Molecular Design Progress in Non-Fullerene Electron Acceptors Towards Commercially Viable Organic Solar Cells. *Chem. Soc. Rev.* **2019**, *48*, 1596–1625.

(15) Anthony, J. E.; Brooks, J. S.; Eaton, D. L.; Parkin, S. R. Functionalized Pentacene: Improved Electronic Properties from Control of Solid-State Order. *J. Am. Chem. Soc.* **2001**, *123*, 9482–9483.

(16) Vehoff, T.; Baumeier, B.; Troisi, A.; Andrienko, D. Charge Transport in Organic Crystals: Role of Disorder and Topological Connectivity. *J. Am. Chem. Soc.* **2010**, *132*, 11702–11708.

(17) Sherman, J. B.; Purushothaman, B.; Parkin, S. R.; Kim, C.; Collins, S.; Anthony, J.; Nguyen, T.-Q.; Chabinyc, M. L. Role of Crystallinity of Non-Fullerene Acceptors in Bulk Heterojunctions. *J. Mater. Chem. A* **2015**, *3*, 9989–9998.

(18) Giri, G.; Verploegen, E.; Mannsfeld, S. C. B.; Atahan-Evrenk, S.; Hwan Kim, D.; Sang Yoon, L.; Becerril, H. A.; Aspuru-Guzik, A.; Toney, M. F.; Bao, Z. Tuning Charge Transport in Solution-Sheared Organic Semiconductors Using Lattice Strain. *Nature* **2011**, *480*, 504–508.

(19) Yao, Z.-F.; Wang, J.-Y.; Pei, J. Control of π-π Stacking via Crystal Engineering in Organic Conjugated Small Molecule Crystals. *Cryst. Growth Des.* **2018**, *18*, 7–15.

(20) Lin, Y.; Zhao, F.; Wu, Y.; Chen, K.; Xia, Y.; Li, G.; Prasad, S. K. K.; Zhu, J.; Huo, L.; Bin, H. et al. Mapping Polymer Donors toward High-Efficiency Fullerene Free Organic Solar Cells. *Adv. Mater.* **2017**, *29*, 1604155.

(21) Han, G.; Guo, Y.; Song, X.; Wang, Y.; Yi, Y. Terminal π-π Stacking Determines Three-Dimensional Molecular Packing and Isotropic Charge Transport in an A–π–A Electron Acceptor for Non-Fullerene Organic Solar Cells. *J. Mater. Chem. C* **2017**, *5*, 4852–4857.

(22) Mondelli, P.; Boschetto, G.; Horton, P. N.; Tiwana, P.; Skylaris, C.-K.; Krompiec, M.; Morse, G. Meta-Analysis: the Molecular Organization of Non-Fullerene Acceptors. *Unpublished manuscript* **2019**,

(23) Few, S.; Frost, J. M.; Kirkpatrick, J.; Nelson, J. Influence of Chemical Structure on the Charge Transfer State Spectrum of a Polymer:Fullerene Complex. *J. Phys. Chem. C* **2014**, *118*, 8253–8261.

(24) Niedzialek, D.; Duchemin, I.; Branquinho de Queiroz, T.; Osella, S.; Rao, A.; Friend, R.; Blase, X.; Kümmel, S.; Beljonne, D. First Principles Calculations of Charge Transfer Excitations in Polymer-Fullerene Complexes: Influence of Excess Energy. *Adv. Funct. Mater.* **2015**, *25*, 1972–1984.

(25) Falke, S. M.; Rozzi, C. A.; Brida, D.; Maiuri, M.; Amato, M.; Sommer, E.; De Sio, A.; Rubio, A.; Cerullo, G.; Molinari, E. et al. Coherent Ultrafast Charge Transfer in an Organic Photovoltaic Blend. *Science* **2014**, *344*, 1001–1005.

(26) Fazzi, D.; Barbatti, M.; Thiel, W. Hot and Cold Charge-Transfer Mechanisms in Organic Photovoltaics: Insights into the Excited States of Donor/Acceptor Interfaces. *J. Phys. Chem. Lett.* **2017**, *8*, 4727–4734.

(27) Ma, H.; Troisi, A. Direct Optical Generation of Long-Range Charge-Transfer States in Organic Photovoltaics. *Adv. Mater.* **2014**, *26*, 6163–6167.

(28) Wouk de Menezes, L. C. and Jin, Y. and Benatto, L. and Wang, C. and Koehler, M. and Zhang, F. and Stolz Roman, L., Charge Transfer Dynamics and Device Performance of Environmentally Friendly Processed Nonfullerene Organic Solar Cells. *ACS Appl. Energy Mater.* **2018**, *1*, 4776–4785.

(29) Shi, J. and Isakova, A. and Abudulimu, A. and van den Berg, M. and Kwon, O.-K. and Meixner, A. J. and Park, S. Y. and Zhang, D. and Gierschner, J. and Lüer, L., Designing High Performance All-Small-Molecule Solar Cells with Non-Fullerene Acceptors: Comprehensive Studies on Photoexcitation Dynamics and Charge Separation Kinetics. *Energy Environ. Sci.* **2018**, *11*, 211–220.

(30) Lin, Y.; Wang, J.; Zhang, Z.-G.; Bai, H.; Li, Y.; Zhu, D.; Zhan, X. An Electron Acceptor Challenging Fullerenes for Efficient Polymer Solar Cells. *Adv. Mater.* **2015**, *27*, 1170–1174.

(31) Shi, X.; Zuo, L.; Jo, S. B.; Gao, K.; Lin, F.; Liu, F.; Jen, A. K.-Y. Design of a Highly Crystalline Low-Band Gap Fused-Ring Electron Acceptor for High-Efficiency Solar Cells with Low Energy Loss. *Chem. Mater.* **2017**, *29*, 8369–8376.

(32) Berny, S.; Blouin, N.; Distler, A.; Egelhaaf, H.-J.; Krompiec, M.; Lohr, A.; Lozman, O. R.; Morse, G. E.; Nanson, L.; Pron, A. et al. Solar Trees: First Large-Scale Demonstration of Fully Solution Coated, Semitransparent, Flexible Organic Photovoltaic Modules. *Adv. Sci.* **2016**, *3*, 1500342.

(33) Skylaris, C.-K.; Haynes, P. D.; Mostofi, A. A.; Payne, M. C. Introducing ONETEP: Linear-Scaling Density Functional Simulations on Parallel Computers. *J. Chem. Phys.* **2005**, *122*, 084119.

(34) Skylaris, C.-K.; Mostofi, A. A.; Haynes, P. D.; Diéguez, O.; Payne, M. C. Nonorthogonal Generalized Wannier Function Pseudopotential Plane-Wave Method. *Phys. Rev. B* **2002**, *66*, 035119.

(35) Mostofi, A. A.; Haynes, P. D.; Skylaris, C.-K.; Payne, M. C. Preconditioned Iterative Minimization for Linear-Scaling Electronic Structure Calculations. *J. Chem. Phys* **2003**, *119*, 8842.

(36) Aldrich, T. J.; Matta, M.; Zhu, W.; Swick, S. M.; Stern, C. L.; Schatz, G. C.; Facchetti, A.; Melkonyan, F. S.; Marks, T. J. Fluorination Effects on Indacenodithienothiophene Acceptor Packing and Electronic Structure, End-Group Redistribution, and Solar Cell Photovoltaic Response. *J. Am. Chem. Soc.* **2019**, *141*, 3274–3287.

(37) Perdew, J. P.; Burke, K.; Ernzerhof, M. Generalized Gradient Approximation Made Simple. *Phys. Rev. Lett.* **1996**, *77*, 3865–3868.

(38) Grimme, S. Semiempirical GGA-Type Density Functional Constructed with a Long-Range Dispersion Correction. *J. Comput. Chem.* **2006**, *27*, 1787–1799.

(39) Ratcliff, L.; Hine, N. D. M.; Haynes, P. D. Calculating Optical Absorption Spectra for Large Systems Using Linear-Scaling Density Functional Theory. *Phys. Rev. B* **2011**, *84*, 165131.

(40) Zuehlsdorff, T. J.; Hine, N. D. M.; Payne, M. C.; Haynes, P. D. Linear-Scaling Time-Dependent Density-Functional Theory Beyond the Tamm-Dancoff Approximation: Obtaining Efficiency and Accuracy with *in situ* Optimised Local Orbitals. *J. Chem. Phys.* **2015**, *143*, 204107.

(41) Materials Studio, version 8.0; software for simulating and modeling materials, Dassault Systèmes BIOVIA. 2016; San Diego, CA.

(42) Frisch, M. J.; Trucks, G. W.; Schlegel, H. B.; Scuseria, G. E.; Robb, M. A.; Cheeseman, J. R.; Scalmani, G.; Barone, V.; Mennucci, B.; Petersson, G. A. et al. Gaussian 09, Revision D.01. 2013; Gaussian Inc.: Wallingford, CT.

(43) Becke, A. D. Density-Functional Thermochemistry. III. The Role of Exact Exchange. *J. Chem. Phys.* **1993**, *98*, 5648.

(44) Stephens, P. J.; Devlin, F. J.; Chabalowski, C. F.; Frisch, M. J. Ab Initio Calculation of Vibrational Absorption and Circular Dichroism Spectra Using Density Functional Force Fields. *J. Phys. Chem.* **1994**, *98*, 11623–11627.

(45) Weigend, F.; Ahlrichs, R. Balanced Basis Sets of Split Valence, Triple Zeta Valence and Quadruple Zeta Valence Quality for H to Rn: Design and Assessment of Accuracy. *Phys. Chem. Chem. Phys.* **2005**, *7*, 3297–3305.

(46) Weigend, F. Accurate Coulomb-Fitting Basis Sets for H to Rn. *Phys. Chem. Chem. Phys.* **2006**, *8*, 1057–1065.

(47) Graham, K. R.; Cabanetos, C.; Jahnke, J. P.; Idso, M. N.; El Labban, A.; Ngongang Ndjawa, G. O.; Heumueller, T.; Vandewal, K.; Salleo, A.; Chmelka, B. F. et al. Importance of the Donor:Fullerene Intermolecular Arrangement for High-Efficiency Organic Photovoltaics. *J. Am. Chem. Soc.* **2014**, *136*, 9608–9618.

(48) Pan, Q.-Q.; Li, S.-B.; Wu, Y.; Sun, G.-Y.; Geng, Y.; Su, Z.-M. A Comparative Study of a Fluorene-Based Non-Fullerene Electron Acceptor and $PC_{61}BM$ in an Organic Solar Cell at a Quantum Chemical Level. *RSC Adv.* **2016**, *6*, 81164.

(49) Clarke, T. M.; Durrant, J. R. Charge Photogeneration in Organic Solar Cells. *Chem. Rev.* **2010**, *110*, 6736–6767.

(50) Brabec, C. J.; Gowrisanker, S.; Halls, J. J. M.; Laird, D.; Jia, S.; Williams, S. P. Polymer-Fullerene Bulk-Heterojunction Solar Cells. *Adv. Mater.* **2010**, *22*, 3839–3856.

(51) Lee, J.; Vandewal, K.; Yost, S. R.; Bahlke, M. E.; Goris, L.; Baldo, M. A.; Manca, J. V.; Van Voorhis, T. Charge Transfer State Versus Hot Exciton Dissociation in Polymer-Fullerene Blended Solar Cells. *J. Am. Chem. Soc.* **2010**, *132*, 11878–11880.

(52) van der Hofstad, T. G. J.; Di Nuzzo, D.; van den Berg, M.; Janssen, R. A. J.; Meskers, S. C. J. Influence of Photon Excess Energy on Charge Carrier Dynamics in a Polymer-Fullerene Solar Cell. *Adv. Energy Mater.* **2012**, *2*, 1095–1099.

(53) Vandewal, K.; Albrecht, S.; Hoke, E. T.; Graham, K. R.; Widmer, J.; Douglas, J. D.; Schubert, M.; Mateker, W. R.; Bloking, J. T.; Burkhard, G. F. et al. Efficient Charge Generation by Relaxed Charge-Transfer States at Organic Interfaces. *Nat. Mater.* **2014**, *13*, 63–68.

(54) Yan, C. and Barlow, S. and Wang, Z. and Yan, H. and Jen, A. K.-Y. and Marder, S. R. and Zhan, X., Non-Fullerene Acceptors for Organic Solar Cells. *Nat. Rev. Mater.* **2018**, *3*, 18003.

(55) Athanasopoulos, S.; Schauer, F.; Nádaždy, V.; Weiß, M.; Kahle, F.-J.; Scherf, U.; Bässler, H.; Köh;er, A. What is the Binding Energy of a Charge Transfer State in an Organic Solar Cell? *Adv. Energy Mater.* **2019**, *9*, 1900814.

(56) Bakulin, A. A.; Rao, A.; Pavelyev, V. G.; van Loosdrecht, P. H. M.; Pshenichnikov, M. S.; Niedzialek, D.; Cornil, J.; Beljonne, D.; Friend, R. H. The Role of Driving Energy and Delocalized States for Charge Separation in Organic Semiconductors. *Science* **2012**, *335*, 1340–1344.

(57) Boschetto, G.; Krompiec, M.; Skylaris, C.-K. Insights into the Charge-Transfer Mechanism of Organic Photovoltaics: Effect of Domain Size. *J. Phys. Chem. C* **2018**, *122*, 17024–17034.

Graphical TOC Entry